DESIGN OF A PROTON SUPERCONDUCTING LINAC FOR A NEUTRON SPALLATION SOURCE

T. P. WANGLER, J. H. BILLEN, K. R. CRANDALL*, J.P.KELLEY, F. KRAWCZYK, S. NATH, H. PADAMSEE[+], D. L. SCHRAGE, and R. VALICENTI.

Los Alamos National Laboratory, Los Alamos, NM 87545 USA
*TechSource, Santa Fe, NM 87594-1057
[+]Laboratory of Nuclear Studies, Cornell University, Ithica, NY 14853

Abstract

We describe the design of a pulsed superconducting linac that accelerates a 2-mA average current beam of H^- ions from 0.2 to 1 GeV. This design would replace the normal-conducting linac design of the pulsed, 6% duty factor US Spallation Neutron Source (SNS) with superconducting cavities above an energy of about 200 MeV. The design takes advantage of the large velocity acceptance of the superconducting cavities to cover the velocity range from about 200 MeV to 1 GeV with only two elliptical cavity shapes. Comparing this design with the baseline 805-MHz normal-conducting design, the superconducting design saves 33 out of 60 2.5-MW klystrons, reduces the overall length of 465 m by 100 m, and reduces the ac power by about 10 MW. We describe the design procedures including the choices of the basic parameters, design of the cavity shapes, and beam dynamics and mechanical analyses.

1 INTRODUCTION

Superconducting linear accelerators are considered an option for pulsed neutron-spallation-source projects in Europe, Japan, and the US. Advantages include reductions in ac power, in linac length because of the higher accelerating gradients, and in the number of klystrons and associated rf power systems. Furthermore, there is an increased safety margin against radioactivation from beam losses that would impede hands-on-maintenance and would limit the availability. This latter advantage is the result of the higher gradients that increase the longitudinal focusing, larger bore radius that becomes economically possible, and the improved vacuum in the cryogenic environment of the superconducting accelerator.

Recent advances in rf superconducting technology have addressed important technical issues for a pulsed superconducting injector linac, including demonstration at the TESLA Test Facility (TTF) of pulsed electron beam operation at high accelerating gradients[1,2], and at other laboratories higher power input couplers[3,4], and elliptical cavities[5,6,7] for lower velocity beams. Rf control issues for proton superconducting linacs have also been studied.[8] These developments present spallation-neutron-source projects with an opportunity for a high-performance superconducting linac, especially at the higher velocities (β>0.4).

A normal-conducting linac for low-velocity particles combined with a superconducting linac for high-velocity particles utilizes the advantages of both technologies. High-current, low-velocity proton linacs have demanding focusing requirements to control space-charge forces, which can be provided straightforwardly with present normal-conducting structures. But, focusing requirements relax with increasing velocity and are compatible with the longer-period focusing lattice of a high-velocity superconducting linac. Because of the widespread experience with elliptical cavities for velocity-of-light particles (electrons), the elliptical-cavity geometry can be used with confidence at the high-velocity end of the linac. Then, for linacs in the 1-GeV energy range, the advantages of the superconducting linac are realized for the main portion of the machine.

In this paper we describe the design of a pulsed superconducting linac that accelerates a 2-mA average current beam of H^- ions from 0.2 to 1 GeV. The proton superconducting linac will be comprised of a number of sections, each of which uses a periodic array of normal-conducting quadrupole magnets, and superconducting cavities with identical shapes. The cavities are designed to perform over the given velocity range and are identified by a design velocity called the geometric velocity or β_G, which for a π-mode structure is nominally twice the cell length divided by the free space rf wavelength. For a superconducting linac that accelerates relativistic electrons, there is only one constant-β_G section, and β_G =1.

The parameters are chosen consistent with our design objectives. Generally, these are: 1) Provide for maximum klystron power utilization to minimize the cost of the rf system. 2) Maximize the fraction of cavities able to achieve the accelerating gradient and peak surface fields. 3) Provide acceptable beam-dynamics performance. 4) Minimize the total accelerator length. 5) Minimize the number of constant-β_G sections to reduce the overall cavity-development effort. These five objectives cannot all be satisfied simultaneously, and the best that can be done is to find an acceptable compromise.

Although the specific design that will be presented in this paper was produced for the US Spallation Neutron

Source (SNS) project, it is not the only superconducting linac design that was considered for the project. For the design presented here, decisions and parameter choices were intended to provide the maximum benefits from the rf superconducting technology at lowest cost, and consistent with a minimal schedule impact for the project, which already had a baseline normal-conducting linac design. For example, we chose to retain an existing baseline SNS normal-conducting design below about 200 MeV. This design uses 2.5-MW, 805-MHz klystrons that had already been chosen for the project, which implies that each klystron will drive more than one cavity. The cavity design uses a large number of cells (8 cells) per cavity to reduce the number of cavities and associated components, such as rf input power couplers. The design uses a small number (two) of distinct elliptical cavity shapes. The superconducting linac parameter choices, particularly the accelerating gradients and rf input power-coupler levels, were based on performance that had already been demonstrated in an accelerator with beam rather than simply in a laboratory test configuration.

2 ARCHITECTURE DESIGN

Determination of the architecture is the first stage of the design process. To begin, one needs to determine the β_G values of the cavities, the number of constant-β_G sections, and the beam-velocity limits for each section. The multicell cavity transit-time factor $T(\beta)$ as a function of particle velocity is needed for this step. As a first approximation, an analytic model of multicell π-mode cavities, made up of cells with an accelerating gap of length g, is used to provide an expression for $T(\beta)$. The model is based on a simple cavity-field distribution with a uniform axial electric field in the accelerating gaps. The field abruptly falls to zero immediately outside the gaps. For a cavity with N identical cells, $T(\beta)$ can be expressed as a product of two separate factors, $T(\beta)=T_G T_S$. The gap factor T_G, which is also the transit-time factor for a single gap of length g, rf wavelength λ, and particle-velocity β, is given by the expression $T_G = \sin(\pi g/\beta\lambda)/(\pi g/\beta\lambda)$. The synchronism factor T_S is a function of N and of the ratio of the local velocity, β, to the cavity geometric velocity, $\beta_G = 2L/\lambda$, where L is the gap spacing. The synchronism factor is given by:

$$T_S = \begin{Bmatrix} (-1)^{\frac{N-1}{2}} \cos(N\pi\beta_G/2\beta)/N\cos(\pi\beta_G/2\beta), N\,\text{odd} \\ (-1)^{\frac{N}{2}+1} \sin(N\pi\beta_G/2\beta)/N\cos(\pi\beta_G/2\beta), N\,\text{even} \end{Bmatrix} \quad (1)$$

Equation 1 has been compared with direct numerical computations of $T(\beta)$ for elliptical-cavity cell shapes. We found that to obtain better agreement with our cavity shapes, we must modify the velocity dependence in the model to account for penetration of the fields into the beam pipe at the end cells. We replaced $g=0.463\beta_G\lambda$ in the expression for T_G, and replaced β_G by $1.04\beta_G$ in Eq.1.

First, a trial value for the number of cells per cavity N is chosen. Then Eq.1 is used to specify the approximate velocity range over which the cavities will be used. The velocity range is specified by Eq.1 in terms of β_{min}/β_G and β_{max}/β_G, where β_{min} and β_{max} are the minimum and maximum section velocities. The choices for these limiting values are determined by the fraction that, at the ends of each section, the transit time factor is allowed to decrease from its maximum value. If the accelerating gradient is chosen conservatively enough, a practical value for the transit-time factor at the ends of each section is in the approximate range of 75% to 80%T_{MAX}.

The procedure starts with the known final velocity and works backwards using the values of β_{min}/β_G and β_{max}/β_G to determine β_{min}, β_{max}, and β_G for each section until the input energy is reached. When the values of β_G and N are determined, an electromagnetic field-solver code such as SUPERFISH[9] can be used to calculate more accurate numerical values of the cavity parameters.

The next step in the architecture design is to determine the accelerating gradient, which is related to the rf power delivered to the cavity. Generally, the RF power delivered to the beam greatly exceeds the power dissipated in the superconducting walls. Then, the so-called peak rf power delivered to each cavity, P_C, is accurately given by the peak beam power, which is equal to the product of the beam current times the particle energy gain ΔW per cavity. In our design procedure ΔW is held constant for all cavities within a given section. The peak power is given by

$$P_C = I\Delta W/q = IE_0 T(\beta)\cos(\phi)N\beta_G\lambda/2 \quad (2)$$

The beam current I is averaged over an RF period, ϕ is the design phase of the field when the beam centroid is at the center of a cavity, and E_0 is the integral of the axial electric field divided by the nominal active length of the cavity, $\lambda = N\beta_G\lambda/2$. The value of ϕ at this stage of the design process may not be final, since ϕ will be used later to obtain longitudinal beam matching as will be discussed in the next section. The quantity E_A, usually called the accelerating gradient in the superconducting rf literature, is given by $E_A=E_0T_{MAX}$, where $T_{MAX}=T(\beta_T)$, and where the velocity β_T gives the maximum transit-time factor. It is more common for proton linacs to express the energy gain and beam power in terms of E_0 rather than E_A. The velocities, β_T and β_G , are not exactly equal because of the gap factor T_G, which increases with increasing particle velocity. Given the values of I, ϕ, N, β_G, λ, and transit-time factors from Eq.1, Eq.2 relates $E_0T(\beta)$ to P_C. Usually, P_C is determined by the available rf power per cavity.

An economically attractive design option at the present time is to use klystrons that have an available rf power P_{kly} large enough to drive more than one cavity. The available power is what remains after control margin

and waveguide losses have been included. Using Eq.2, P_{kly} determines the product E_0TN_{cav} for each section, where N_{cav} is the number of cavities driven by each klystron. N_{cav} can be chosen to provide an operating value for E_0T that corresponds to a safe value for the peak surface fields. The number of cavities per cryomodule can be chosen to provide a practical cryomodule length and, when the focusing is provided by normal-conducting quadrupoles between the cryomodules, a quadrupole-focusing period that is short enough to satisfy the beam focusing requirement. P_{kly} can be adjusted as required to set any desired transition energy between the normal and superconducting linacs. After making these choices, the initial values of the rf input power per cavity, the energy gain per cavity, the number of cryomodules, the input and output energies for each section, and the total number of cavities, cryomodules, and klystrons for each section are determined. If the total length of a full spatial period, including the cryomodule and the quadrupole magnets between cryomodules, is determined from a detailed mechanical layout, since the number of periods is known, the total physical length of the superconducting linac is determined.

Assuming a value of Q_0 (We have assumed a conservative value of $3X10^9$.), the niobium rf wall-power dissipation P_{wall} is obtained for each cavity, where P_{wall} varies throughout each section, because E_0 (and $E_A=E_0T_{MAX}$) varies. We must provide cooling, not only because of the cavity wall-power dissipation, but also because of additional heat inputs within the cryomodule, including the radiation shields, supports, rf power from higher-order modes, and both static and rf heat inputs for the rf power couplers. Based on a thermal analysis of a similar cryomodule from a previous project,[10] we can obtain good estimates for the cryomodule cooling requirements. Finally, we include heat inputs for the cryogenic distribution system between the refrigerator and the linac.

We assume that the cavities are cooled at 2 K, and that the power couplers and shields are cooled serially with supercritical flow entering at 4.5 K. Conservatively assuming an 8% rf duty factor, we can estimate the cryomodule dynamic heat loads. No additional margin is applied to the cavity loads, and a 40% margin is assigned to all other loads (couplers, shields, supports, etc...). To these values are added the heat loads for the distribution system, where we use 0.5 W/m for the 2 K circuit, and 1.9 W/m for the coupler/shield circuit,[11] and where each circuit has a supply and return equal to the length of the accelerator plus 50 m to allow for variability in cryoplant location.[12,13] An additional safety factor of 1.2 is used for refrigeration control. For comparison purposes, the loads of the two circuits are related to an equivalent load at 4.5 K using the Carnot relationship, and efficiencies of 0.16 and 0.23 for the 2 K and 4.5 K circuits, respectively.

3 BEAM DYNAMICS DESIGN

The beam-dynamics design determines the quadrupole lattice and gradients to satisfy the transverse beam-dynamics requirements, and determines the cavity phases to satisfy the longitudinal beam-dynamics requirements. Strong focusing is needed to balance the defocusing space-charge force, and keep the beam size small. Strong transverse focusing is realized by maintaining a large transverse phase advance per unit length, and usually the preferred lattice is one that provides the shortest spatial period. For a superconducting linac with normal-conducting quadrupoles located between cryomodules, a doublet lattice is preferred because it provides a shorter period than a singlet lattice.

The main parameters in each section are determined in the architecture design stage; in particular, for each section the architecture design determines the energy gain per cavity ΔW_{cav}, the period length L, and the number of cavities per klystron and per cryomodule. The quadrupole gradients are usually chosen to provide the strongest transverse focusing, while avoiding the envelope instability[14]. The gradients may also be constrained by the requirement that the space-charge tune depression ratios in all planes should be greater than about 0.4 to avoid possible chaos that is observed in beam-halo models. The particle motions in the three planes are coupled; thus, if the transverse focusing is too strong, the 0.4 requirement could be difficult to satisfy longitudinally. The quadrupole gradients are not uniquely specified. For example, one could choose the gradients to equipartition the beam. In the high-energy linac this choice usually has the disadvantage of weakening the transverse focusing and increasing the transverse beam size. However, the chosen solution at the design stage is not critical since the quadrupole gradients are adjustable, and experimental optimization is possible.

At each interface between different focusing lattices, the gradients of the last two quadrupoles of the upstream section and the first two quadrupoles of the downstream section are adjusted to provide a transverse match. If the transverse phase-advance per unit length is kept constant across the interface, the beam will still be matched even if the beam current changes.

The longitudinal focusing depends on the cavity phases and on $E_0T(\beta)$, which is determined for each section at the architecture design stage. Before we define the cavity phase we must first define the cell phase. The phase for any cell is defined as the phase of the accelerating field when the beam centroid arrives at the electrical center of the cell. The electrical center is nearly the same as the geometric center for an inner cell, but these centers can deviate appreciably for an outer cell because of field leakage into the attached beam pipe. For an outer cell the location of the electrical center can be calculated numerically. For an odd number of cells per cavity, the cavity phase is defined as the phase of the center cell. For an even number of cells per cavity, the cavity phase is defined as the average of the phases of the two center cells.

The choice of cavity design phase represents a compromise between operation on the crest of the rf waveform to provide the most efficient acceleration, and operation earlier than the crest to provide longitudinal

focusing. Usually, the economic advantage of efficient acceleration dictates that the cavity phase should not deviate from the crest by much more than about 30 degrees, and operating very close to the crest results in inadequate longitudinal focusing in proton machines.

Nevertheless, it always desirable to choose the cavity phases to provide longitudinal matching at the transitions between the normal and superconducting linacs and between the different sections of the superconducting linac. Within each section the design phase is ramped linearly. The matching criterion between sections is $(\Delta W_{cryo}/L)\tan(\phi)$ where ΔW_{cryo} is the energy gain per cryomodule. The matching criterion maintains the same longitudinal focusing strength on both sides of the interface, and provides a longitudinal match, even if the current varies. Since ΔW_{cryo} and L are different for each section, ϕ will generally change abruptly at the interface. Although it would not be necessary in principle, we keep the design phases the same for all cavities in the same cryomodule. After the matching between interfaces and the linear phase ramping within each section are defined, the design phases are determined for every cavity.

The values of E_0 for the cells of each cavity are calculated in a design code. The program uses two nested loops, an outer loop that determines E_0 and an inner loop that determines the cavity input phase ϕ_{in}, such that the design values of the cavity phase and the energy gain are obtained. For the detailed dynamics, transit-time factors are used that correspond to individual cells rather than the whole cavity. The parameters that are needed for the calculation are the velocity-dependent inner-cell and outer-cell transit-time factors T_{in}, and T_{out}, the offset of the outer-cell electrical center from its geometric center, and the ratio of E_0 values of the outer to the inner cells. Two different values of E_0 are used, one for the inner cells, and one for the two outer cells.

The phase loop uses ϕ_{in} equal to the design phase for the initial guess, and the initial value for E_0 is determined from the design cavity energy gain. The centroid is stepped cell by cell through the cavity. At the electrical center of each cell, the centroid receives an energy kick. Between adjacent electrical centers separated by a distance d, the centroid phase is advanced according to $\Delta\phi = 2\pi d/\beta\lambda$, where β is the centroid velocity. For an even number of cells per cavity, the phases of the two center cells are averaged to give the cavity phase for comparison with the cavity design phase ϕ. Then ϕ_{in} is modified and the process is repeated until the cavity phase equals the design value.

After the phase loop has converged, the energy gain through the whole cavity, which is the sum of the energy gains over each cell, is compared with the design cavity energy gain. If these do not agree, E_0 is adjusted and the process is repeated until the design energy gain is obtained.

4 LINAC DESIGN

Using the method described above, we have produced a design concept for a 1-GeV, 2-MW H^- linac (Fig.1) consisting of a normal-conducting proton linac to 194.3 MeV, followed by an 805-MHz pulsed superconducting linac. The superconducting linac accelerates the beam using two distinct 8-cell elliptical superconducting-cavity shapes, designed with cell lengths corresponding to two different geometric beta values β_G=0.61 and 0.76 (Fig.2). A summary of some of the parameters is shown in Table 1. The mean accelerating gradient, averaged over all cavities, is E_A=9.6 MV/m, and the mean values of peak surface fields are B_{peak}=50 mT and E_{peak}=28 MV/m.

The rf system uses 2.5-MW klystrons to drive ten β_G =0.61 cavities or six β_G =0.76 cavities. The rf-control system uses both feedback and feedforward for the control of the vector sum of the fields from all the cavities that are driven by a given klystron. The alternative concept is to drive each cavity with its own rf source, which allows control of the individual phases and amplitudes of each cavity, but is expected to be more costly.

Figures 3 through 13 show different aspects of the design. Shown are drawings of the two cryomodule layouts (Fig. 3), energy gain per cavity (Fig.4), cavity transit-time factors (Fig.5), accelerating gradient (Fig.6), peak surface electric field (Fig.7), peak surface magnetic field (Fig.8), external Q (Fig.9), peak surface field distribution compared with scaled TESLA TTF measured distribution (Fig.10), cavity wall power losses (Fig.11), beam sizes and aperture radii (Fig.12), and transverse rms normalized emittances (Fig.13). In particular, the design accelerating gradients should be achievable, and the beam-dynamics requirements for transverse beam size and emittance are satisfied.

One may wonder whether operation at velocities far from β_G might cause large longitudinal emittance growth, associated with a large cell-to-cell variation of the phase throughout the five cells of a cavity. For this design, we found that the maximum beam-phase slip between the first and eighth cells, occurring for the cavities at the section ends, was well over 100 degrees (see Table 2). Nevertheless, the beam-dynamics simulations showed no significant effects caused by this phase slip. We found that the results from our detailed cell-by-cell treatment are indistinguishable from the simpler approach of calculating the dynamics using a single equivalent gap, and using the phase of the middle cell[15].

An initial study was carried out of linac energy centroid jitter, which for 99.99% of the time is required to be within 2.2 MeV of the design value. Based on 1000 simulation runs with random phase and amplitude errors induced by microphonic frequency variations of ±25 Hz, and with rf control errors of ±0.5% amplitude and ±0.5 deg phase for the vector sum, the centroid energy jitter extended beyond the required limit to about ±3 MeV. The conclusion is that if the microphonics are that large, some form of feedback would be required to control the jitter.

Table 1. Superconducting Linac Parameters

Parameter	β_G=0.61 section	β_G=0.76 section	Total
Cells per cavity	8	8	
Aperture radius [mm]	50	50	
$ZT(\beta_G)^2/Q_0$[Ω/m]	354	498	
T_{MAX}	0.726	0.734	
E_{PK}/E_A	3.65	2.75	
B_{PK}/E_A[mT/MV/m]	1.73	1.76	
W_{min}[MeV]	194.3	355.4	
W_{max}[MeV]	355.4	1000.0	
ΔW per cavity[MeV]	5.37	8.95	
Cavity beam power [kW]	193	322	
Lattice period length[m]	4.5	7.0	
Cavities/cryomodule	2	3	
Cryomodules/klystron	5	2	
Number cavities	30	72	102
Number cryomodules	15	24	39
Number klystrons	3	12	15
Total length[m]	68	168	236
Ave Nb wall loss [W]	145	516	661
2 K cryomodule heat load per section [W]	237	730	967
2 K distribution system heat load [W]			282
2 K total load with 1.2 safety factor [W]			1498
Coupler/shield heat load [W]	1335	3012	4347
Coupler/shield distribution system heat load [W]			1094
Coupler/shield total load with 1.2 safety factor [W]			6529
Equivalent load at 4.5 K [W]*			7054

* Assumes a refrigerator return temperature of 34 K for the coupler/shield circuit. Performing this calculation for the original CEBAF cryoplant, one finds that this cryoplant is roughly half that size.

Table 2. Design phases at the end cavities of the two sections in the superconducting SNS design.

β_G	cavity	ϕ_1 (deg)	ϕ_8 (deg)	ϕ_8- ϕ_1 (deg)
0.60	first	-82.9	+38.3	+121.7
0.60	last	+29.7	-93.4	-123.1
0.75	first	-96.9	+40.1	+137.0
0.75	last	+49.8	-104.3	-154.1

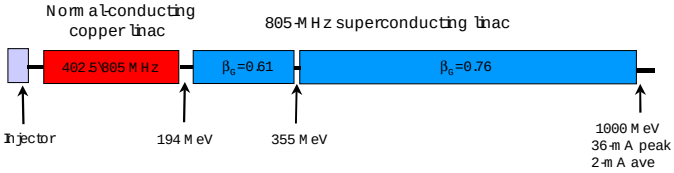

Figure 1. Block diagram of the linac.

5 CAVITY DESIGN

Each cavity structure consists of eight cells operating in the π mode. One would like a large number of cells per cavity to reduce the number of rf drives and the number of rf windows. However, for a given cell-to-cell coupling, increasing the number of cells per cavity degrades the field stability. The bore radius of 5.0 cm gives an intercell coupling factor of about k=2%, which we believe will produce acceptable field errors in the 8-cell cavities. An 8-cell cavity has six identical internal cells plus the two end cells. The end cells have beam pipes attached and therefore are necessarily different than the internal cells. The shape of the inner half wall of an end cell is chosen to be the same as that of an internal cell. The outer half wall is allowed a different shape for proper tuning. In addition, the beam pipes at each end of the cavity are larger than the internal bore radius to help achieve sufficient coupling to the rf power source. Previous work has shown that a beam-pipe radius of about 5.5 cm is adequate. Cavity shapes[16] are shown in Fig. 2.

Either of two phenomena may limit the performance of a superconducting cavity, quench or electron field emission. Designing the cavity for minimum E_{peak}/E_A will minimize field emission in the cavity, but does not necessarily lead to the best cavity performance, because this may result in a cavity that is limited by quench. It is thus important to limit the peak magnetic field (B_{peak}). So, E_{peak}/E_A is minimized while B_{peak}/E_{peak} is constrained. For guidance in the design process, we apply the experience to date in achieving high fields. We use the maximum magnetic and electric fields (B_{max} and E_{max}) that have been achieved experimentally for elliptical cavities. Then, for a particular cavity design, we compute the ratio B_{peak}/E_{peak}. If $B_{peak}/E_{peak} > B_{max}/E_{max}$, then we assume the cavity is more likely to be limited by quenching and if $B_{peak}/E_{peak} < B_{max}/E_{max}$ the cavity is more likely to be limited by field emission. Assuming the peak field limitations observed for the TESLA cavities, we have chosen the ratio B_{max}/E_{max} =120 mT/70 MV/m = 1.71 mT/(MV/m).

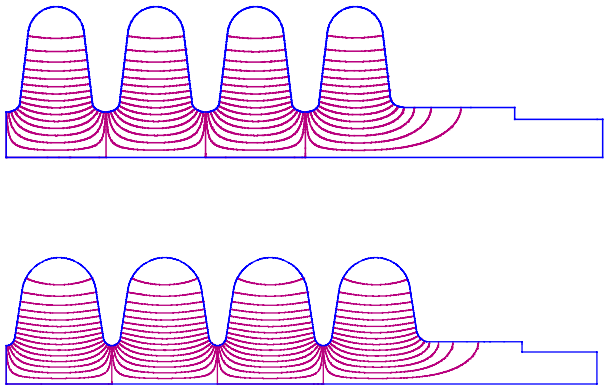

Figure 2. SUPERFISH generated cavity shapes for β_G= 0.61 (top) and β_G = 0.76 (bottom) for half of an 8-cell cavity. The contour lines correspond to constant values of the magnetic field H_ϕ. The electric field is parallel to these contours.

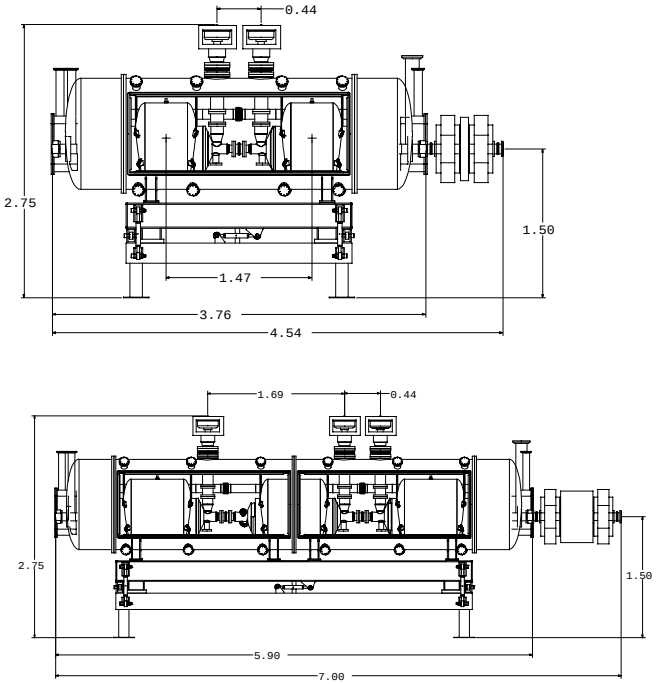

Figure 3. Cryomodule period with two β_G=0.61 cavities (above) and three β_G=0.76 cavities (below) followed by a room-temperature quadrupole doublet behind the cryomodule.

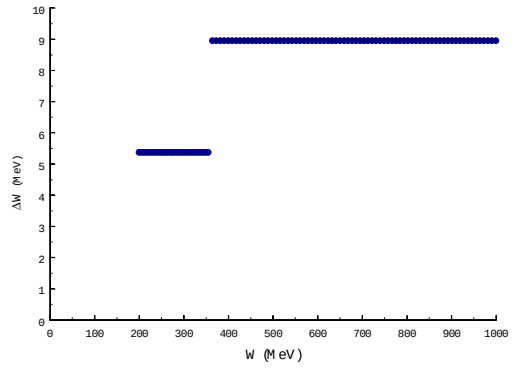

Figure 4. Energy gain per cavity versus energy.

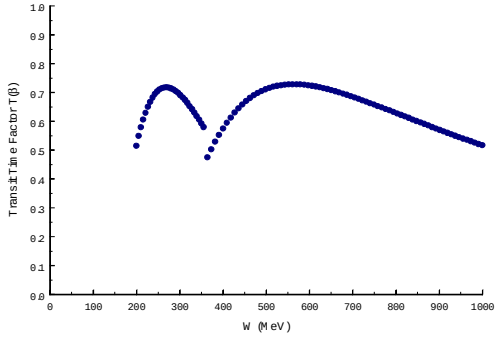

Figure 5. Cavity transit-time factor versus energy.

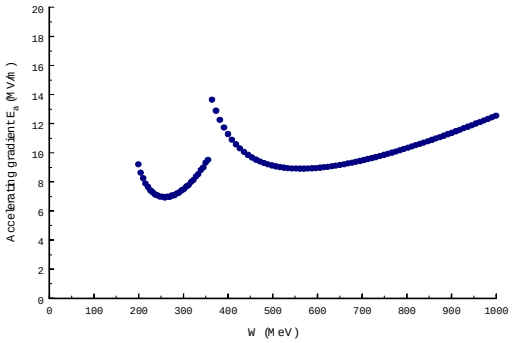

Figure 6. Accelerating gradient versus energy.

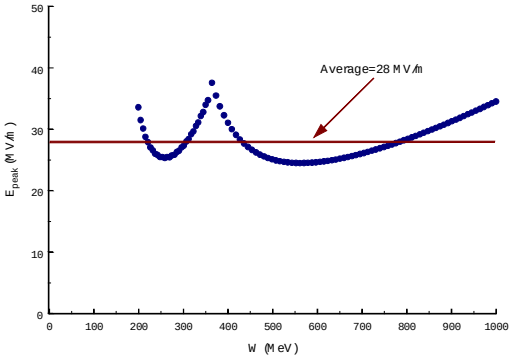

Figure 7. Peak surface electric field versus energy.

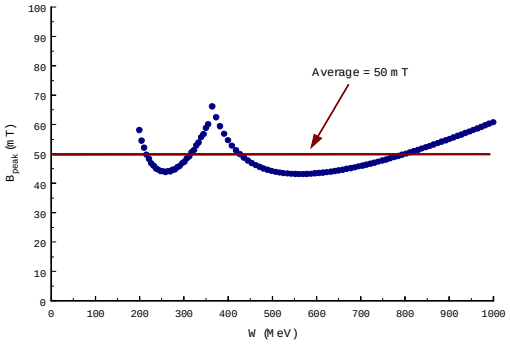

Figure 8. Peak surface magnetic field versus energy.

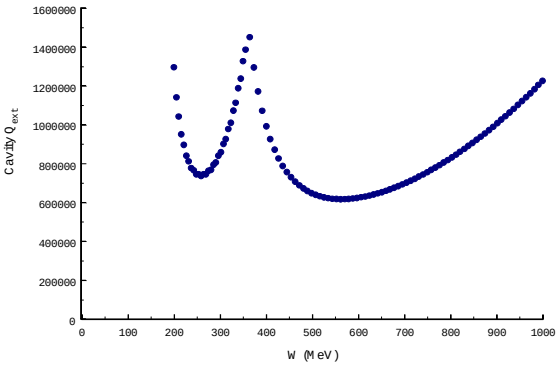

Figure 9. External quality factor versus energy.

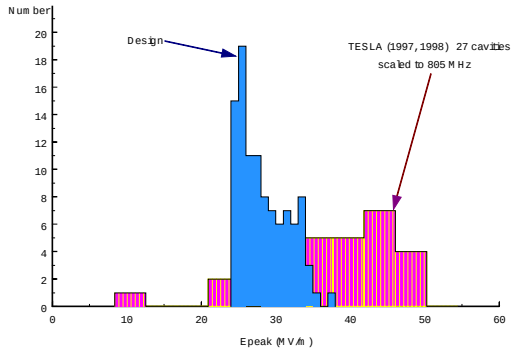

Figure 10. Design peak surface electric field distribution compared with TESLA measured peak surface fields scaled to 805 MHz using a surface area to the one fourth power scaling.

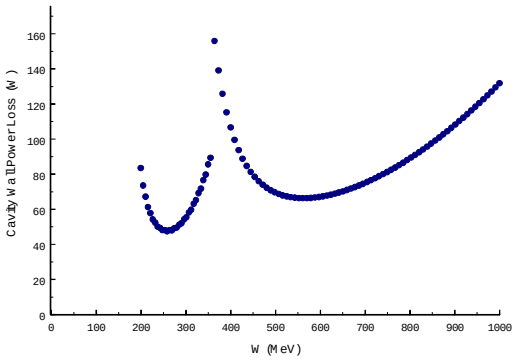

Figure 11. Cavity wall power loss versus energy.

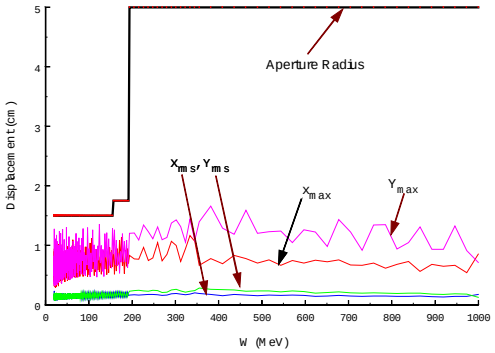

Figure 12. Energy variation of maximum and rms beam projections from 10k particle linac simulation through the whole linac including linac errors. Also shown is the aperture radius for comparison.

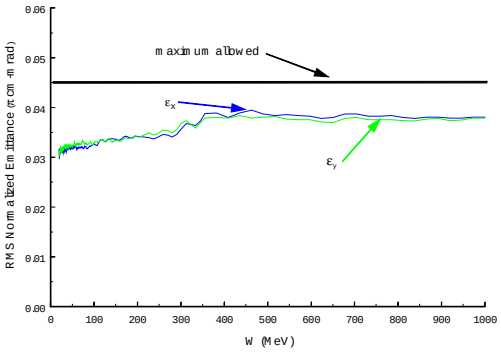

Figure 13. Transverse rms normalized emittances versus energy. The maximum allowed emittance requirement determined by the accumulator ring is shown for comparison.

6 LORENTZ FORCE AND MICROPHONIC EFFECTS

The higher Q values for superconducting cavities means that the phases and amplitudes are more sensitive to cavity resonant frequency variations than is the case for normal-conducting cavities. The two issues of greatest concern are Lorentz-force detuning and microphonics. Lorentz-force detuning[17] is caused by the small deformations of the cavity walls in response to pressure

from the time-average rf electric and magnetic forces. This electromagnetic pressure causes the resonant frequency to shift by an amount Δf, which is typically several hundred Hertz. The steady-state value of the frequency shift is small, and generally can be compensated by a mechanical tuner. However, the cavity mechanical structure cannot respond instantly to a pulse of electromagnetic energy, and consequently, there is a transient variation of the cavity resonant frequency over a typical time scale of order about 1 millisecond, together with a corresponding variation of the cavity phases and amplitudes. This transient effect is sometimes called dynamic Lorentz-force detuning. For millisecond-scale pulsed applications, such as a spallation-source linac, compensation must be provided if the phase and amplitude variations are large. The Lorentz coefficient k_L is a measure of the sensitivity of a cavity to this loading, and is defined by $\Delta f = k_L (E_a)^2$. Based on initial estimates, we have tried to restrict the magnitude of the calculated Lorentz coefficient to about $|k_L| < 2.0$ Hz/(MV/m)^2. The cavity design issues for achieving this result are described in the following section.

Initial simulations of the performance of the rf control system have been carried out to evaluate the effects of Lorentz-force detuning, assuming $|k_L| = 2.0$ Hz/(MV/m)^2. The initial results were encouraging, showing that the control of the average phase and amplitude for the cavities within an rf module in the range of ±1 degree and ±1% was achievable, and that the additional rf power required was a small value of only about 2 kW.

Another important effect, known as microphonics, is the excitation of mechanical modes from common sources of vibration in the laboratory. The sources of microphonic excitation may be either random or periodic; typical causes include mechanical pumps and pressure variations in the helium cryostat. The main concern here is with low-frequency mechanical resonant modes, especially with frequencies much lower than about 60 Hz. Microphonics cause rf resonant frequency errors, and phase errors that are greater than they would be in a typical electron linac. This is because for a proton or ion linac, the beam must arrive at the cavity earlier than the crest to provide phase focusing. As a result, to compensate for beam loading the cavity resonant frequency must be higher than the driving frequency. Driving the cavity at a frequency different than the resonant frequency makes the phase more sensitive to resonant frequency errors.

7 MECHANICAL ANALYSIS OF CAVITIES

The two cavities for this design were analyzed with respect to their mechanical properties[18]. The material thickness selected was 3.5 mm as a compromise among structural performance, ease of fabrication, and cost. A summary of the parameters of the two cavity designs is given in Table 3. The structural considerations are the Lorentz coefficient, the mechanical structural resonances, the tuning forces, and the stress under vacuum loading. The first two items dictated that the cavities be stiffened by annular rings in the fashion of the TTF cavities. Without the stiffener rings, the predicted Lorentz coefficient of the $\beta_G = 0.61$ cavity would be –3.5 Hz/(MV/meter)^2, and the lowest mechanical resonance of the $\beta_G = 0.76$ cavity would be less than 10 Hz. It is important to minimize the predicted Lorentz coefficient, as the realities of the stiffnesses of tuning mechanisms and cryostats are such that the magnitudes of Lorentz coefficients measured on LANL and TTF are as high as twice the predicted values. Similarly, the mechanical resonant frequencies were predicted for cavities without rf power couplers, rf pickup ports, and HOM couplers. The presence of such items, coupled with the structural behavior of the cryostat, will serve to reduce the mechanical resonant frequencies.

The presence of the stiffener rings also significantly reduces the stresses due to vacuum loading. Although the stiffener rings do increase the tuning forces, the predicted values are quite satisfactory.

Table 3. Parameters of Superconducting Cavities Fabricated from 3.5 mm-Thick Material.

PARAMETER	$\beta_G = 0.61$	$\beta_G = 0.76$
Iris bore radius (cm)	5.0	5.0
Wall slope (degrees)	7.0	9.0
Mechanical resonant Frequencies (Hz)	$\geq$ 119 Hz	$\geq$ 133 Hz
Lorentz coeff., k_L Hz/(MV/m)^2	-2.1	-1.0
Tuning sensitivity lb/kHz	0.48	1.01
Vacuum loading lb/in^2	2078	2618

8 CONCLUSIONS

We have carried out a design of a pulsed superconducting linac that accelerates a 2-mA average current beam of H^- ions from 0.2 to 1 GeV. This design is based on recent advances in rf superconducting technology, and would replace the normal-conducting linac for the US Spallation Neutron Source (SNS) with superconducting cavities above an energy of about 200 MeV. The superconducting design would save 33 out of 60 2.5-MW klystrons, would reduce the overall length of 465 m by 100 m, and would reduce the ac power by about 10 MW.

9 ACKNOWLEDGMENTS

The authors acknowledge support from the U.S. Department of Energy, and valuable discussions with D. Proch, N. Ouchi, H. Safa, and T. Tajima.

REFERENCES

[1] M. Pekeler,"Experience with Superconducting Cavity Operation in the TESLA Test Facility,"Proc. of the 1999 Particle Accelerator Conference, Mar 29 –Apr 2, 1999, New York, 245.
[2] A.Gamp, S.Goloborodko, A.Kholodnyi, M.Liepe, T.Plawski, K.Rehlich, T.Schilcher, S.N.Simrock, Y.Tchernoousko, and M.Huning,"Experience with the Control of the Vector Sum at the TESLA Test Facility," European Part. Accel. Conf. EPAC98, 22-26 June, 1998, Stockholm, 1738.
[3] S.Mitsunobu, T.Furuya, Y.Kijima, T.Tajima, and T.Tanaka, "High Power Input Coupler for KEKB SC Cavity," these proceedings.
[4] B. Haynes, F. L. Krawczyk, E. Schmierer, D. C. Gautier, J. Gioia, M. A. Madrid, R. E. Lujan, K. C. D. Chan, and B. Rusnak, "High-Power Coaxial Coupler Design and Testing,"these proceedings.
[5] W.B. Haynes, B. Rusnak, K.C.D. Chan, F. Krawczyk, A. Shapiro, R. Bibeau, R. Gentzlinger, D. Montoya, and H. Safa, "Medium-Beta Superconducting Cavity Tests at Los Alamos National Lab for High-Current, Proton Accelerators," Proc. of the 8th Workshop an RF Superconductivity, Abano Terme, Italy,
October 1997, 523.
[6] N. Ouchi, J. Kusano, N. Akaoka, B. Fechner, K. Hasegawa, S. Takeuchi, M. Mizumoto, K. Saito, S. Noguchi, M. Ono, E. Kako and H. Inoue, K. Mukugi, and Y. Honda, "R&D Activities for Superconducting Proton Linac at JAERI,"Asian Part. Accel Conf., APAC98, Tsukuba, Japan, March 1998, 77.
[7] H. Safa, "Superconducting Proton Linac for Waste Transmutation", these proceedings.
[8] M.Huning, S.N.Simrock, and T.Schilcher, "Requirements for the RF Control of the Vector Sum for Superconducting Proton Linacs," Proc. XIX Int. Linear Accel. Conf., Aug.23-28, 1998, Chicago, 543.
[9] J.H.Billen and L.M.Young, "Poisson Superfish", Los National Laboratory report LA-UR-96-1834 (October 31, 1999).
[10] J. Waynert,"Preliminary Estimates of APT Cryomodule Loads,"Los Alamos National Laboratory Tech Note, ESA-EPE: 99.029, (November 6, 1998).
[11] J.P.Kelley,"SRF History: CEBAF and Cryosystem Heat Loads,"Los Alamos National Laboratory Tech Note, LANSCE-1: 98-045, (February 7, 1998).
[12] J.P.Kelley,"Refrigeration Cost Estimate for a Superconducting High Energy Linac for SNS,"Los Alamos National Laboratory Tech Note, LANSCE-1: 99-080, (April 27, 1999).
[13] J.P.Kelley,"Refrigeration Cost Estimate for a Superconducting High Energy Linac for SNS-Addenda,"Los Alamos National Laboratory Tech Note,LANSCE-1: 99-098, (May 14, 1999).
[14] I.Hofmann, L.J.Laslett, L.Smith, and I.Haber, "Stability of the Kapchinskij-Vladimirsky (K-V) Distributions in Long Periodic Transport Systems," Particle Accelerators 13, 145 (1983).
[15] K.R.Crandall, "Comparison of Some LINAC Results", Los Alamos National Laboratory report LA-UR-99-4373, (July 30, 1999).
[16] J.H.Billen,"Superconducting Cavity Design for SNS," Los Alamos National Laboratory internal memorandum, LANSCE-1:99-148 (August, 1999).
[17] E. Haebel and J. Tuckmantel,"Electromagnetic Surface Forces on RF Cavities,"CERN AT-RF(Int)-91-999 (December, 1999).
[18] D. Schrage, "Structural Analysis of Superconducting Cavities," Los Alamos National Laboratory report, LA-UR/99-5826 (November, 1999).